



Universiteit  
Leiden  
The Netherlands

## **Methane formation in cold regions from carbon atoms and molecular hydrogen**

Lamberts, A.L.M.; Fedoseev, G.; Hemert, M.C. van; Qasim, D.N; Chuang, K.; Carvalho Santos, J. de; Linnartz, H.V.J.

### **Citation**

Lamberts, A. L. M., Fedoseev, G., Hemert, M. C. van, Qasim, D. N., Chuang, K., Carvalho Santos, J. de, & Linnartz, H. V. J. (2022). Methane formation in cold regions from carbon atoms and molecular hydrogen. *The Astrophysical Journal*, 928(1).  
doi:10.3847/1538-4357/ac51d1

Version: Publisher's Version  
License: [Creative Commons CC BY 4.0 license](https://creativecommons.org/licenses/by/4.0/)  
Downloaded from: <https://hdl.handle.net/1887/3514165>

**Note:** To cite this publication please use the final published version (if applicable).



# Methane Formation in Cold Regions from Carbon Atoms and Molecular Hydrogen

Thanja Lamberts<sup>1,2</sup> , Gleb Fedoseev<sup>2,3</sup> , Marc C. van Hemert<sup>1</sup>, Danna Qasim<sup>2,4</sup> , Ko-Ju Chuang<sup>2</sup> , Julia C. Santos<sup>2</sup> , and Harold Linnartz<sup>2</sup>

<sup>1</sup>Leiden Institute of Chemistry, Gorlaeus Laboratories, Leiden University, P.O. Box 9502, 2300 RA Leiden, The Netherlands; [a.l.m.lamberts@lic.leidenuniv.nl](mailto:a.l.m.lamberts@lic.leidenuniv.nl)

<sup>2</sup>Laboratory for Astrophysics, Leiden Observatory, Leiden University, P.O. Box 9513, 2300 RA Leiden, The Netherlands

<sup>3</sup>Research Laboratory for Astrochemistry, Ural Federal University, Kuibysheva St. 48, 620026 Yekaterinburg, Russia

Received 2021 September 16; revised 2022 January 18; accepted 2022 February 2; published 2022 March 25

## Abstract

Methane is typically thought to be formed in the solid state on top of cold interstellar icy grain mantles via the successive atomic hydrogenation of a carbon atom. In the current work we investigate the role of molecular hydrogen in the CH<sub>4</sub> reaction network. We make use of an ultrahigh vacuum cryogenic setup combining an atomic carbon atom beam with atomic and/or molecular beams of hydrogen and deuterium on a water ice. These experiments lead to the formation of methane isotopologues detected in situ through reflection absorption infrared spectroscopy. Most notably, CH<sub>4</sub> is experimentally formed by combining C atoms with only H<sub>2</sub> on amorphous solid water, albeit more slowly than in experiments where H atoms are also present. Furthermore, CH<sub>2</sub>D<sub>2</sub> is detected in an experiment involving C atoms with H<sub>2</sub> and D<sub>2</sub> on H<sub>2</sub>O ice. CD<sub>4</sub>, however, is only formed when D atoms are present in the experiment. These findings have been rationalized by means of computational and theoretical chemical insights. This leads to the following conclusions: (a) the reaction C + H<sub>2</sub> → CH<sub>2</sub> takes place, although it is not barrierless for all binding sites on water, (b) the reaction CH + H<sub>2</sub> → CH<sub>3</sub> is barrierless, but has not yet been included in astrochemical models, (c) the reactions CH<sub>2</sub> + H<sub>2</sub> → CH<sub>3</sub> + H and CH<sub>3</sub> + H<sub>2</sub> → CH<sub>4</sub> + H can take place only via a tunneling mechanism, and (d) molecular hydrogen possibly plays a more important role in the solid-state formation of methane than assumed so far.

*Unified Astronomy Thesaurus concepts:* Astrochemistry (75); Interstellar molecules (849); Molecular spectroscopy (2095); Molecular clouds (1072); Laboratory astrophysics (2004); Computational methods (1965)

## 1. Introduction

Methane, the smallest hydrocarbon, is one of the few molecules that have been detected in the solid phase in various regions in the interstellar medium (Boogert et al. 2015). In fact, the first detection was a simultaneous gas-phase and tentative solid-phase identification, based on the  $\nu_4$  feature at 7.6  $\mu\text{m}$  (Lacy et al. 1991); meanwhile several in-depth observational studies have been reported (Boogert et al. 1996; Öberg et al. 2008). Early reports based on comparison to laboratory data indicated that methane likely resides in ice comprising polar component(s) (Boogert et al. 1996), and it was later postulated that H<sub>2</sub>O is the primary candidate for this based on correlations between CH<sub>4</sub> and H<sub>2</sub>O column densities (Öberg et al. 2008). This points to the fact that solid CH<sub>4</sub> is formed during the translucent phase of the evolutionary track of molecular clouds.

The solid-state formation of methane has typically been assumed to follow four sequential atomic hydrogenation steps of the carbon atom in the <sup>3</sup>P ground state ever since this was postulated in the late 1940s (van de Hulst 1946, 1949; D’Hendecourt et al. 1985; Brown et al. 1988; Brown & Charnley 1991). Recently, this route has been confirmed experimentally (Qasim et al. 2020a) through the simultaneous use of well-characterized C- and H-atom beams, following up

on early work by Hiraoka et al. (1998):



The hydrogen atom number density in molecular clouds is estimated to be around a few atoms cm<sup>-3</sup>, which is two to four orders of magnitude lower than the molecular hydrogen abundance depending on whether a translucent or dense cloud is concerned (van Dishoeck & Black 1988; Goldsmith & Li 2005). Therefore, solid-state reactions with molecular hydrogen can also be of great importance even when the corresponding rate constants are lower, as pointed out already by Hasegawa & Herbst (1993). For instance, for the sequential hydrogenation of the O atom to eventually form water (Hiraoka et al. 1998; Ioppolo et al. 2008; Miyauchi et al. 2008) it has been shown that the reaction H<sub>2</sub> + OH → H<sub>2</sub>O + H can become more relevant than H + OH → H<sub>2</sub>O even though a considerable barrier is invoked (Cuppen & Herbst 2007; Furuya et al. 2015). Another example is the hydrogenation of carbon monoxide by UV irradiation of mixed CO:H<sub>2</sub> ices (Chuang et al. 2018). Despite such active involvement of H<sub>2</sub> in solid-state reactions, the molecular hydrogen abundances on ice surfaces in astrochemical microscopic models are often artificially reduced to save (a lot of) computational cost, e.g., by decreasing the sticking coefficient (Garrod 2013; Lamberts et al. 2013; Vasyunin & Herbst 2013). We also want to point out that, despite the fact that neutral carbon atoms are often thought to only be (abundantly) present in translucent regions (van Dishoeck & Black 1988; Snow & McCall 2006), there

<sup>4</sup> Current address: Astrochemistry Laboratory, NASA Goddard Space Flight Center, Greenbelt, MD 20771, USA.



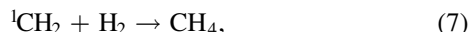
Original content from this work may be used under the terms of the [Creative Commons Attribution 4.0 licence](https://creativecommons.org/licenses/by/4.0/). Any further distribution of this work must maintain attribution to the author(s) and the title of the work, journal citation and DOI.

exists substantial literature that indicates that C [I] is more extended, possibly even into denser regions (Langer 1976; Keene et al. 1985; Papadopoulos et al. 2004; Burton et al. 2015; Bisbas et al. 2019).

For these reasons, we consider a number of reactions with molecular hydrogen in the context of methane formation. First, the direct addition or insertion reactions:

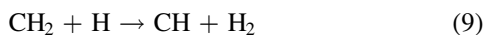
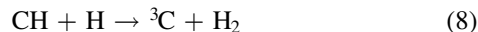


Reaction (5), the first step in the reaction network, has been covered in a series of papers indicating that the reaction may readily take place in helium droplets (Krasnokutski et al. 2016; Henning & Krasnokutski 2019), and including this reaction in astrochemical models without a barrier was suggested recently (Simončič et al. 2020). The reaction



intuitively the most likely step to form methane, can only take place if methylene is in the excited singlet state,  ${}^1\text{CH}_2$  (Murrell et al. 1973; Bauschlicher et al. 1977). In the system currently under study experimentally, only ground-state  ${}^3\text{CH}_2$  is expected to be present, and therefore reaction (7) will not be further considered. Excited-state singlet carbon atoms can, however, play a role in other interstellar environments, for instance Titan’s atmosphere (Hickson et al. 2016), but this is beyond the scope of the current paper.

In terms of the chemical reaction network, there is furthermore the possibility of hydrogen abstraction, either from  $\text{H}_2$  or from a  $\text{CH}_n$  fragment:



Reactions (8)–(11) are listed in the exothermic direction, and the reverse endothermic reactions are not expected to be important given the low temperatures involved ( $\sim 10$ – $20$  K). We assume that the exothermicities of the reactions are not significantly altered by the solid-state surroundings of the reaction site. This essentially translates into assuming that the binding energies of the reactants and products are similar. We also assume that the H atoms formed in reactions (10) and (11) immediately desorb, based on the argument of conservation of energy and momentum (Koning et al. 2013).

In the current paper, we revisit reaction (5) in water ices and extend the discussion on  $\text{H}_2$  reactivity, investigating the influence of reactions (6)–(11). We show that reactions (5), (10), and (11) together can lead to the formation of methane, without the involvement of H atoms. To achieve this, we make use of in situ infrared spectroscopy to probe which methane isotopologues are formed via reaction of  ${}^3\text{C}$  with selected combinations of atomic and molecular hydrogen (H,  $\text{H}_2$ ) and deuterium (D,  $\text{D}_2$ ) on representative interstellar water-rich ice analogs.

This paper is organized in the following way. The experimental details and results are discussed in Sections 2.1 and 3. Furthermore, we position the chemical network listed above within the context of the extensive theoretical chemical

literature, complemented by additional computations presented that explicitly take into account the role of the water ice surface. This helps to disentangle which reactions are likely to take place throughout the various experiments, as outlined in Section 2.2 and discussed in Section 4. Solid methane is hard to observe from ground-based observatories because of telluric pollution. Observations from space offer an alternative. Solid methane has been observed already with the Spitzer space telescope (Öberg et al. 2008). Because of its higher sensitivity and spatial resolution, the James Webb Space Telescope (JWST) is expected to substantially extend these observations. The present experimental work and theoretical approach fits worldwide efforts to prepare for upcoming JWST observations. In Section 5 the astrochemical implications and conclusions of this work are presented.

## 2. Methodology

### 2.1. Experimental Methodology

The experimental setup used is SURFRESIDE<sup>3</sup>, an ultrahigh vacuum (UHV) system with three atomic beam lines (Ioppolo et al. 2013; Qasim et al. 2020b). For the purpose of our study, only H/ $\text{H}_2$ , D/ $\text{D}_2$ , and C atom beam lines are used. Ices are grown on a gold-coated copper substrate that is attached to the cold finger of a closed-cycle He cryostat in the center of the main UHV chamber with a base pressure of the order of  $10^{-10}$  mbar. Co-deposition experiments of  $\text{H}_2\text{O} + ({}^3\text{P})\text{C}$  and combinations of H, D,  $\text{H}_2$ , and/or  $\text{D}_2$  are performed that lead to the growth of a mixed ice at 10 K. Mixed H/ $\text{H}_2$  or D/ $\text{D}_2$  beams are obtained by (partial) dissociation of molecular  $\text{H}_2$  (Linde 5.0) or  $\text{D}_2$  (Linde 2.8) in a microwave discharge atom source (MWAS, Oxford Scientific, Schmidt et al. 1996; Anton et al. 2000) in a separate vacuum chamber with a base pressure of  $\sim 10^{-9}$  mbar. Note that charged particles are removed by applying an electric field that deflects these species. Excited-state species are de-excited through collisions with the walls of a U-shaped quartz pipe at room temperature placed along the beam path prior to the molecules entering the main chamber. A customized SUKO-A 40 C-atom source (Qasim et al. 2020b) based on a commercial design (Dr. Eberl, MBE, Krasnokutski & Huisken 2014; Albar et al. 2017) produces a beam of carbon atoms in the  ${}^3\text{P}$  ground state, albeit with a mean translational kinetic energy of the order of the source temperature ( $\sim 2000$  K), with a  $C_n/C$  ( $n > 1$ ) ratio of less than 0.01. Based on recent calculations for the energy dissipation timescale of less than a few picoseconds for translationally hot nitrogen atoms on amorphous solid water, we expect no impact of the high carbon source temperature on the possible chemistry that takes place (Molpeceres et al. 2020). This source is located in another separate vacuum chamber with a base pressure  $(3\text{--}5) \times 10^{-9}$  mbar. A series of apertures is used to collimate the C-atom beam on the substrate, avoiding deposition of carbon on the walls of the main UHV chamber. Note that CO and  $\text{CO}_2$  are known contaminants in the C-atom beam. A third vacuum chamber with a base pressure of  $\sim 10^{-9}$  mbar is used to generate a molecular  $\text{H}_2\text{O}$  (Milli-Q) or  $\text{D}_2\text{O}$  (Sigma-Aldrich, 99.9 at.% D) beam for simultaneous deposition (molecular deposition line, MDL). We use an overabundance of  $\text{H}_2\text{O}$  to mimic a polar ice environment, e.g., in agreement with the previously mentioned correlation between observed  $\text{CH}_4$  and  $\text{H}_2\text{O}$  column densities. Water reaches the surface with a translational kinetic energy equal to or less than room

**Table 1**  
List of Experimental Conditions (Temperature, Flux, Mixing Ratio and Time), Organized into Four Selected Sets

#	$T$ (K)	$\text{H}_2\text{O}$ ( $\text{cm}^{-2} \text{s}^{-1}$ )	$\text{C}$ ( $\text{cm}^{-2} \text{s}^{-1}$ )	$\text{H}$ ( $\text{cm}^{-2} \text{s}^{-1}$ )	$\text{H}_2$ ( $\text{cm}^{-2} \text{s}^{-1}$ )	$\text{D}$ ( $\text{cm}^{-2} \text{s}^{-1}$ )	$\text{D}_2$ ( $\text{cm}^{-2} \text{s}^{-1}$ )	C:H:H <sub>2</sub> :D:D <sub>2</sub>	Time (min)
		MDL	SUKO	MWAS	MWAS		MDL		
1 A	10	$8 \times 10^{12}$	$5 \times 10^{11}$	$2 \times 10^{12}$	$1 \times 10^{14}$			1:4:200:--	30
1 B	10	$8 \times 10^{12}$	$5 \times 10^{11}$	$2 \times 10^{12}$	$1 \times 10^{14}$		$1 \times 10^{13}$	1:4:200:--:20	30
1 C	10	$8 \times 10^{12}$	$5 \times 10^{11}$	$2 \times 10^{12}$	$1 \times 10^{14}$		$4 \times 10^{13}$	1:4:200:--:80	30
		MDL	SUKO		MDL	MWAS	MWAS		
2 A	10	$8 \times 10^{12}$	$5 \times 10^{11}$			$1.5 \times 10^{12}$	$6 \times 10^{13}$	1:--:--:3:120	30
2 B	10	$8 \times 10^{12}$	$5 \times 10^{11}$		$5 \times 10^{13}$	$1.5 \times 10^{12}$	$6 \times 10^{13}$	1:--:100:3:120	30
2 C	10	$8 \times 10^{12}$	$5 \times 10^{11}$		$2 \times 10^{14}$	$1.5 \times 10^{12}$	$6 \times 10^{13}$	1:--:400:3:120	60
		MDL	SUKO		MDL		MDL		
3 A	10	$1.2 \times 10^{13}$	$5 \times 10^{11}$				$1 \times 10^{14}$	1:--:--:--:200	60
3 B	10	$1.2 \times 10^{13}$	$5 \times 10^{11}$		$1 \times 10^{14}$		$1 \times 10^{14}$	1:--:200:--:200	240
#	$T$ (K)	$\text{D}_2\text{O}$ ( $\text{cm}^{-2} \text{s}^{-1}$ )	$\text{C}$ ( $\text{cm}^{-2} \text{s}^{-1}$ )		$\text{H}_2$ ( $\text{cm}^{-2} \text{s}^{-1}$ )				Time (min)
		MDL	SUKO		MDL				
4 A	<b>10</b>	$1.4 \times 10^{13}$	$5 \times 10^{11}$		$2.5 \times 10^{14}$			1:--:500:--:--	60
4 B	<b>25</b>	$1.4 \times 10^{13}$	$5 \times 10^{11}$		$2.5 \times 10^{14}$			1:--:500:--:--	60

**Note.** MDL, SUKO, and MWAS refer to the atomic and molecular deposition lines used (see text). Furthermore the substrate temperature, the atomic and molecular fluxes, and the total time of the experiment, from which the fluence can be derived, are listed. All fluxes give the effective value. Note that H ( $\text{H}_2$ ) and D ( $\text{D}_2$ ) have different thermal velocities and sticking coefficients, thus a direct comparison should be made with care. Values in bold font underline the different settings within one series of measurements.

temperature. Based on the lack of dangling modes in the infrared spectra, we conclude that the co-deposition of C, H/ $\text{H}_2$ , and  $\text{H}_2\text{O}$  does not lead to the deposition of a very porous amorphous solid water ice. The atomic and molecular fluxes are listed in Table 1, in which all experiments are summarized. The uncertainty in the flux determination is roughly a factor of two. The initial reactants and formed products are monitored in situ via reflection absorption infrared spectroscopy (RAIRS, Greenler 1966) in the solid state. Note that the infrared beam is guided toward and from the entrance and exit windows of the chamber via boxes that are purged with dry air to reduce atmospheric absorption. Finally, a baseline correction is performed that includes the subtraction of known components of the purging gas used along the path of the infrared beam, i.e., outside the vacuum chamber, such as water vapor. The experiments are organized into four different series in which relevant parameters are systematically varied—see Table 1.

## 2.2. Computational Methodology

The primary focus of our own calculations is on the reaction  $\text{C} + \text{H}_2 \rightarrow \text{CH}_2$ , since it is the first and most determining step in the reaction network mentioned above leading to  $\text{CH}_4$ . Moreover, the carbon atom is known to be highly reactive (Kim et al. 2003). However, with the exception of the work by Simončič et al. (2020), to date it has not been looked at in detail for surface chemistry purposes. Note that for the other possible steps (reactions (6)–(11)), we draw from previous studies available from the literature.

We take a threefold approach—see also Figure 1—to understand the reactivity of  $\text{C} + \text{H}_2 \rightarrow \text{CH}_2$ :

1. a gas-phase calculation of a highly symmetric orientation of C with respect to  $\text{H}_2$  ( $\text{C}_{2v}$  symmetry)—meant to compare against previous results,
2. a gas-phase calculation of a low-symmetry orientation of C with respect to  $\text{H}_2$  ( $\text{C}_s$  symmetry)—meant to be a first step toward a realistic symmetry-broken orientation on a surface,
3. the calculation of the reaction of  $\text{H}_2$  with a C atom bound to a single  $\text{H}_2\text{O}$  molecule and an  $(\text{H}_2\text{O})_3$  cluster (no symmetry)—meant as a first step toward understanding the reaction with a bound carbon atom on a water ice.

When a gas-phase  $\text{H}_2$  molecule approaches a carbon atom in its  $^3\text{P}$  ground state the encounter can occur on three, initially degenerate, potential surfaces (PESs). Important to take into account is the alignment of the two singly occupied 2p orbitals of the carbon atom. When the orientation of the  $\text{H}_2$  molecule is perpendicular to the direction of approach, there is a  $\text{C}_{2v}$  symmetry and the three surfaces are  $^3\text{B}_1$ ,  $^3\text{B}_2$ , and  $^3\text{A}_2$ . For all three surfaces the energy was calculated as a function of the Jacobi coordinates  $R$  as the distance between C and the center of mass of  $\text{H}_2$ ,  $r$  as the H–H distance, and  $\theta = 90^\circ$  as the angle between  $R$  and  $r$ ; see again Figure 1. All calculations were repeated in  $\text{C}_s$  symmetry, where the angle  $\theta$  was reduced to  $80^\circ$ , while keeping the CAS/CI parameters as close as possible to the ones used in the  $\text{C}_{2v}$  case. In  $\text{C}_s$  symmetry two  $^3\text{A}''$  states are relevant. Subsequently, to find possible reaction paths, the location of the crossing (seam) between the  $^3\text{B}_1$  and  $^3\text{A}_2$  for  $\text{C}_{2v}$  and the two  $^3\text{A}''$  surfaces for  $\text{C}_s$  was searched for by scanning these surfaces with small steps in the  $R \approx r \approx 1 \text{ \AA}$  range. These calculations have been performed using Molpro (Werner et al. 2012, 2018) with the AVQZ basis set (Woon & Dunning 1993; Dunning et al. 2001). The CASSCF calculation had eight

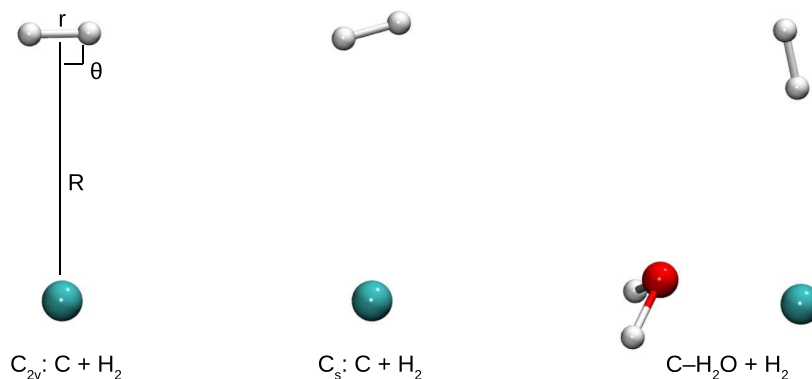


**Figure 1.** Three cases studied for the reaction  $C + H_2 \rightarrow CH_2$ ; the reaction on the  $(H_2O)_3$  cluster is not depicted here.

electrons in eight orbitals, while state-averaging over singlet and triplet states, each with four lowest roots, for both  $C_{2v}$  and  $C_s$  symmetries.

In order to test—for the first time—the influence of the strong adsorption of the carbon atom atop water ice (see also Molpeceres et al. 2021) on the reactivity of the carbon atom with  $H_2$  we have performed a nudged elastic band calculation for the reaction of  $H_2$  with a carbon atom bound to a water molecule, i.e., a  $C-H_2O$  complex, and to a water trimer  $(H_2O)_3$ , i.e., a  $C-(H_2O)_3$  complex. This was followed by a transition state optimization applying the dimer method with the B3LYP functional (Becke 1988, 1993; Lee et al. 1988) and a def2-TZVP basis set (Weigend & Ahlrichs 2005), using DL-find in Chemshell (Kästner et al. 2009; Metz et al. 2014). For the calculations with the single water molecule, single-point energies were calculated for the reactant, transition, and product states, with both MRCI/AVTZ (Werner & Knowles 1988; Dunning 1989; Kendall et al. 1992) and CCSD(T)-F12a/VTZ-F12 (Adler et al. 2007; Peterson et al. 2008; Knizia et al. 2009) in Molpro version 2020 (Werner et al. 2020). All geometries were reoptimized at the CCSD(T)-F12a/VTZ-F12 level of theory in Molpro. MRCI calculations are, in principle, warranted for systems where multiple reference effects can be expected, such as here where a triplet ground state carbon atom is involved. We do note, however, that the  $T1$  and  $D1$  values in both CCSD(T)-F12 calculations are (well) below the common threshold values of  $T1 < 0.04$  and  $D1 < 0.05$  (Janssen & Nielsen 1998; Lambert et al. 2006). Indeed, the MRCI single-point energy calculations indicate that the main contribution of a Slater determinant to the wave function has reference coefficients of about 0.93–0.94 for all  $C-H_2O-H_2$  geometries.

Note that, for the water monomer, all higher level calculations are in good agreement with the energetics predicted by B3LYP/def2-TZVP (see Table 2), and therefore the results for the water trimer are expected to be representative.

### 3. Experimental Results

Figure 2 shows the RAIR spectra of experimental series 1 and 2, over the wavenumber ranges that include all relevant spectroscopic bands of  $CH_4$ ,  $CD_4$ , and  $CH_2D_2$ , indicated by the vertical lines in the figure. Other detected species are listed in Table 4 and discussed in Appendix B.

**Table 2**

Activation and Reaction Energies in  $\text{kJ mol}^{-1}$ ,  $E_{\text{act}}$  and  $E_{\text{react}}$  Respectively, for the Reaction of the  $C-(H_2O)_n$  Complex with  $H_2$  Leading to the  $CH_2-(H_2O)_n$  Complex, with Respect to the Pre-reactive Complex

	B3LYP	MRCI/ B3LYP	CCSD(T)-F12/ B3LYP	CCSD (T)-F12
$E_{\text{int}, C-H_2O}$	-52.9			-36.1
$E_{\text{act}, H_2 \dots C-H_2O}$	30.4	30.0	27.3	30.4
$E_{\text{react}, CH_2-H_2O}$	-294.3	-281.5	-303.1	-300.5
$E_{\text{int}, CH_2-H_2O}$	-8.0			-7.1
$E_{\text{int}, C-(H_2O)_3}$	-95.2			
$E_{\text{act}, H_2 \dots C-(H_2O)_3}$	77.9			
$E_{\text{react}, CH_2-(H_2O)_3}$	-250.9			
$E_{\text{int}, CH_2-(H_2O)_3}$	-9.2			

**Note.** The interaction energy,  $E_{\text{int}}$  of the  $CH_2-(H_2O)_n$  complex is also given, with respect to the separated radical and water cluster. Note that zero-point energies are not included.

Experiments 1A and 2A (top and bottom lines in Figure 2) serve as a control experiment and can be directly compared to previous work (Qasim et al. 2020a). Indeed the formation of  $CH_4$  and  $CD_4$  is clearly confirmed by the presence of both the  $\nu_3$  and  $\nu_4$  vibrational modes. Molecular deuterium (hydrogen) is introduced in experiment 1B (2B) and increased in experiment 1C (2C), and a concomitant decrease of  $CH_4$  ( $CD_4$ ) can be easily observed. At the same time, several  $CH_2D_2$  absorption features appear in these four experiments, with the most intense peak at  $1028 \text{ cm}^{-1}$ . Experiment 1C shows the most apparent, multiline detection of doubly deuterated methane as a result of the advantageous ratio between all reactants:  $C:H:H_2:D_2 = 1:4:200:80$ , see Table 1.

Because doubly deuterated methane is observed in experiments for which either hydrogen or deuterium is present only in the molecular form, at least one reaction with a molecular species must take place throughout the course of methane formation. This is further supported by a tentative  $CH_4$  detection at  $1303 \text{ cm}^{-1}$  in experiment 2C, i.e., in an experiment with hydrogen present only in the molecular form.

In fact, this tentative detection was the reason to perform experimental series 3 and 4 to further investigate whether methane indeed can be formed if only molecular forms of

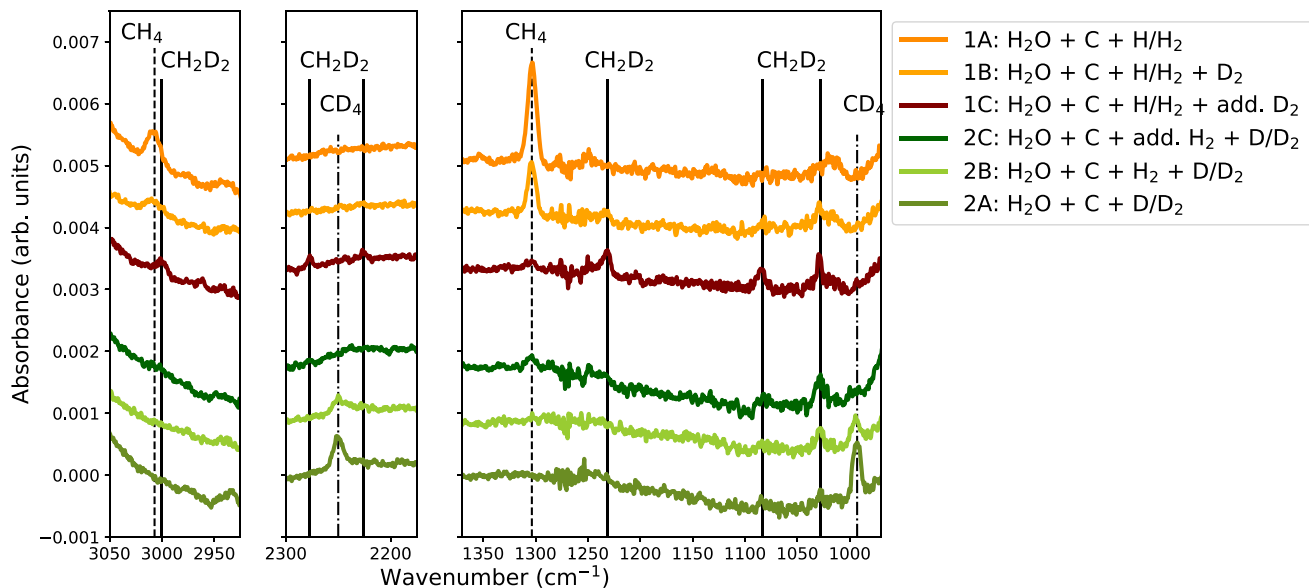


**Figure 2.** RAIR spectra of experimental series 1 and 2; the exact experimental conditions can be found in Table 1. The dashed vertical lines indicate the peak positions of  $\text{CH}_4$ , the solid vertical lines indicate  $\text{CH}_2\text{D}_2$ , and the dashed-dotted lines indicate  $\text{CD}_4$ ; see Table 4 in Appendix B for specific peak positions.

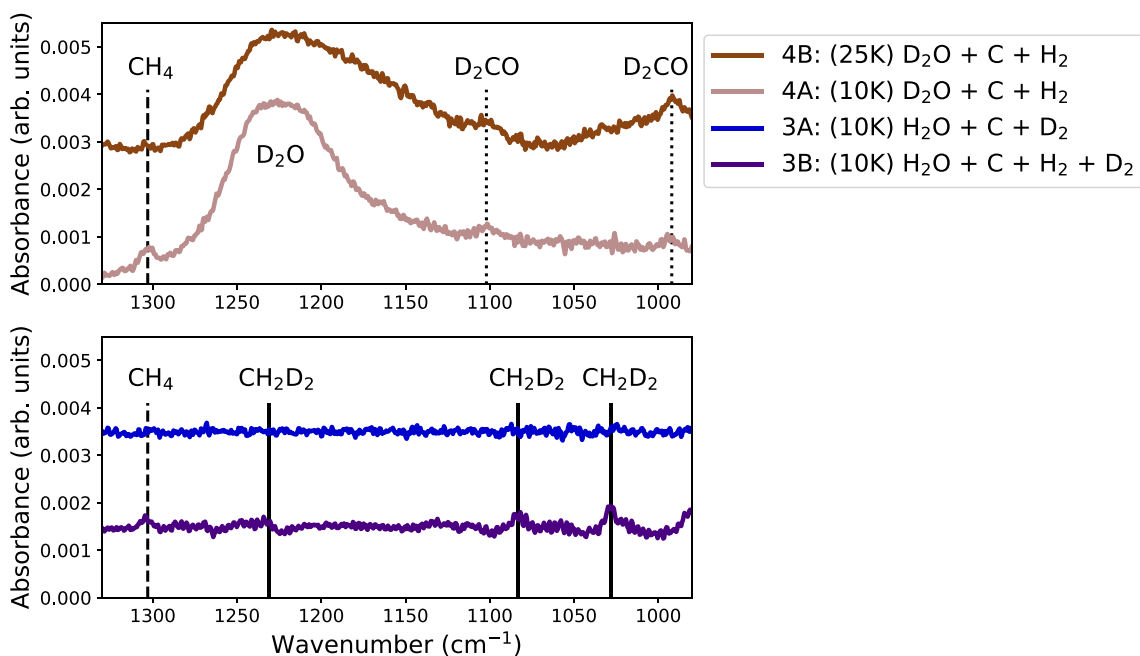


**Figure 3.** RAIR spectra of experiments 3A, 3B, 4A, and 4B; the exact experimental conditions can be found in Table 1. The dashed vertical lines indicate the peak position of  $\text{CH}_4$ , the solid vertical lines indicate  $\text{CH}_2\text{D}_2$ , the dotted lines indicate  $\text{D}_2\text{CO}$ , and the broad peak is caused by  $\text{D}_2\text{O}$  indicated directly in the plot; see Table 4 in Appendix B for specific peak positions.

hydrogen or deuterium are present. In order to increase the signal-to-noise ratio, these experiments have been run over longer times, as indicated in Table 1. The resulting thick ices ( $\sim 200$  ML) and interference patterns over the full range of the IR spectra have led to the presentation of baseline-corrected spectra of a small region of interest only ( $1330\text{--}980$   $\text{cm}^{-1}$ ), depicted in Figure 3.

Experiments 3B, 4A, and 4B clearly result in a lower overall formation rate of methane in comparison to interactions with atomic species. Experiments 3A and 4A represent a

co-deposition of  $\text{C} + \text{D}_2 + \text{H}_2\text{O}$ , and  $\text{C} + \text{H}_2 + \text{D}_2\text{O}$ , respectively. In experiment 3A no  $\text{CD}_4$  is detected, while experiment 4A shows a clear solid-state  $\text{CH}_4$  detection. In other words, in the reaction network for the formation of methane from carbon atoms and molecular hydrogen there is an isotope effect present, which hints at the importance of tunneling in one or more of the involved reactions. Furthermore, experiment 3B, consisting of  $\text{C} + \text{H}_2 + \text{D}_2$  on  $\text{H}_2\text{O}$  ice, shows a clear detection of the two main  $\text{CH}_2\text{D}_2$  peaks at  $1083$  and  $1028$   $\text{cm}^{-1}$ . In other words,  $\text{CH}_2\text{D}_2$  has been formed from carbon atoms and

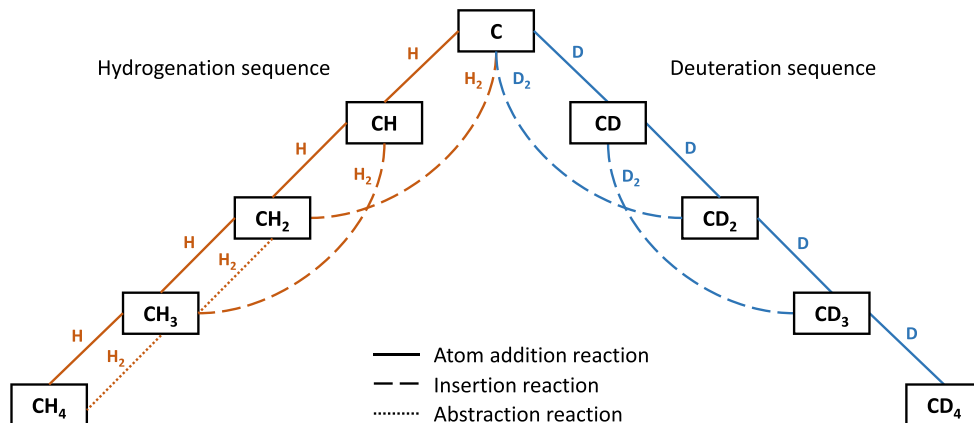


**Figure 4.** Three types of reactions are considered to lead to the formation of  $\text{CH}_4$  or  $\text{CD}_4$ : H or D addition (Qasim et al. 2020a),  $\text{H}_2$  or  $\text{D}_2$  insertion (Krasnokutski et al. 2016; Simončić et al. 2020, and this work), and  $\text{H}_2$  abstraction (this work). We assume that the latter is not efficient with  $\text{D}_2$ , based on the involved high barrier and lack of tunneling efficiency.

molecular species only. However, the yield of  $\text{CH}_2\text{D}_2$  is significantly less than in experiments 1C and 2C.

Experiment 4B, a control experiment, performed at 25 K, i.e., above the desorption temperature of atomic or molecular hydrogen, shows no  $\text{CH}_4$  formation in the solid state, confirming that the processes we are studying take place at the surface at low temperatures.

Finally, no  $\text{CD}_3\text{H}$  or  $\text{CH}_3\text{D}$  was detected in any of the experiments, which can be attributed to a combination of isotope effects, low band strengths, and competition between tunneling and barrierless reactions in the network. A full rationale for the lack of these signals is given in Appendix A.

We can summarize the experimental findings as follows.

1.  $\text{CH}_4$  is detected in experiments on a water ice using both H atoms and  $\text{H}_2$  molecules as well as in experiments using only  $\text{H}_2$ , albeit with a lower efficiency,
2.  $\text{CD}_4$  is detected only in experiments where D atoms are present,
3.  $\text{CH}_2\text{D}_2$  can be detected in experiments that use simultaneously both atomic and molecular hydrogen or deuterium sources,
4.  $\text{CH}_2\text{D}_2$  can also be detected in experiments that use exclusively molecular  $\text{H}_2$  and  $\text{D}_2$ ,
5. Neither  $\text{CH}_3\text{D}$  nor  $\text{CHD}_3$  is detected,
6. All studied reactions take place on the cold ice surface.

#### 4. Theoretical Results

This section focuses on explaining the experimental results by looking in detail at theoretical chemical studies of reactions (5)–(11). Reactions (1)–(4) have been extensively discussed in Qasim et al. (2020a) and will therefore not be further dealt with here. A summary of all relevant reaction steps is depicted in Figure 4.

Section 4.1 contains predominantly results from our own calculations, while Sections 4.2 and 4.3 are based on results available from the literature.

##### 4.1. Reactions on the $\text{CH}_2$ PES

Recently, the reaction  $\text{C} + \text{H}_2 \rightarrow \text{CH}_2$  was proposed to take place readily on interstellar cold surfaces as well (Simončić et al. 2020). We will first review the reaction in the gas phase and then discuss the impact of having a carbon atom bound to a water ice.

All three calculated gas-phase  $\text{C}_{2v}$  surfaces for the  $\text{C} + \text{H}_2$  reaction— ${}^3\text{B}_1$ ,  ${}^3\text{B}_2$ , and  ${}^3\text{A}_2$ —are degenerate for large  $R$  ( $\text{C}-\text{H}_2$  distance) with an energy of  $\sim 330 \text{ kJ mol}^{-1}$  above the  ${}^3\text{B}_1$   $\text{CH}_2$  ground state; see Figure 6 in Appendix C. We find a crossing between the  ${}^3\text{A}_2$  and  ${}^3\text{B}_1$  surfaces at  $R = 1.05 \text{ \AA}$  and  $r = 1.17 \text{ \AA}$  at an energy equal to the asymptotic value of  $\text{C} + \text{H}_2$ . From an energetics point of view and under the assumption that a transition from the  ${}^3\text{A}_2$  to the  ${}^3\text{B}_1$  occurs via a conical intersection, there is no barrier, in agreement with Gamallo et al. (2012). However, at the (avoided) crossing of the  $\text{C}_{2v}$  potential energy surfaces, there is a change in electron configuration. The dominant contribution to the wave function on the  ${}^3\text{A}_2$  surface consists of an occupation for the six valence electrons of  $(2a_1)^2 (3a_1)^2 (1b_1)^1 (1b_2)^1$ , and this needs to change to  $(2a_1)^2 (3a_1)^1 (1b_1)^1 (1b_2)^2$  before reaching the  ${}^3\text{B}_1$   $\text{CH}_2$  ground state. This means an electron has to move from a  $p_z$  orbital on the carbon atom into a  $p_y$  orbital, which can impede the reaction from taking place, even if energetically there is no barrier.

When the symmetry is lowered to  $\text{C}_s$ , which should more closely resemble the situation on an ice surface, by giving up the perpendicular orientation and instead choosing  $\theta = 80^\circ$ , both the  ${}^3\text{B}_1$  and  ${}^3\text{A}_2$  surfaces become of the same  ${}^3\text{A}''$  symmetry and a reaction can take place without a serious energetic barrier. A small hump can be found along the path at  $R = 1.08 \text{ \AA}$  and  $r = 1 \text{ \AA}$ , but this remains below the  $\text{C} + \text{H}_2$  asymptotic value; see Figure 6. Yet the electron configuration still changes upon decreasing  $R$  and increasing  $r$ , i.e., reacting toward  $\text{CH}_2$ , and it is unclear what the effect on the reaction efficiency is.

More importantly, however, the known strong interaction of a  ${}^3\text{P}$  carbon atom with a water molecule or cluster (Wakelam et al. 2017; Shimonishi et al. 2018; Duflo et al. 2021;

Molpeceres et al. 2021) might drastically change the energetics of the reaction. Table 2 gives an overview of the interaction energy of the C–H<sub>2</sub>O complex and the activation and reaction energy of the reaction  $\text{H}_2 + \text{C–H}_2\text{O} \rightarrow \text{CH}_2\text{–H}_2\text{O}$  for different levels of theory. A sizable barrier of 27–30 kJ mol<sup>−1</sup> is found, which certainly cannot be trivially overcome at 10 K. For the reaction in the vicinity of the water trimer, the carbon atom is more strongly bound, by  $\sim 42$  kJ mol<sup>−1</sup>, which is directly reflected in a higher barrier of 77 kJ mol<sup>−1</sup>, i.e.,  $\sim 48$  kJ mol<sup>−1</sup> higher than for the single water molecule. This demonstrates that while the C + H<sub>2</sub> reaction proceeds barrierlessly in helium droplets (Krasnokutski et al. 2016; Henning & Krasnokutski 2019), on water surfaces it will be strongly dependent on the carbon atom binding site. Estimates of the interaction or binding energy depend on the number of water molecules considered and the method used, but generally vary between  $\sim 35$  and  $\sim 130$  kJ mol<sup>−1</sup>, much larger than a typical water hydrogen bond of  $\sim 22$  kJ mol<sup>−1</sup>. Our proof-of-principle calculation demonstrates that more extensive work should be done on C–(H<sub>2</sub>O)<sub>n</sub> clusters with  $n > 3$ . At present, therefore, we cannot elaborate on the expected isotope effect of this reaction, but we expect that this reaction on a water ice proceeds with an (effective) barrier and might thus be slower with D<sub>2</sub> than with H<sub>2</sub>.

Note that reaction (8),  $\text{CH} + \text{H} \rightarrow {}^3\text{C} + \text{H}_2$ , has to proceed through a CH<sub>2</sub> intermediate, as can be seen in Figure 2 of Gamallo et al. (2012). While this is a realistic scenario in gas-phase experiments in the low-pressure regime where intermediates can convert the reaction energy into internal energy to overcome subsequent barriers, such intermediates are expected to be quenched on a surface by rapid ( $< 1$  ps) energy dissipation to a water ice (Fredon et al. 2021). Therefore, reaction (8) turns effectively into reaction (5) on a surface.

#### 4.2. Reactions on the CH<sub>3</sub> PES

The exchange reaction  $\text{CH} + \text{H}_2 \rightleftharpoons \text{CH}_2 + \text{H}$  has been previously studied in the gas phase (McIlroy & Tully 1993; Medvedev et al. 2006; González et al. 2011). In particular, Medvedev et al. (2006) showed that the reaction proceeds through an activated CH<sub>3</sub><sup>\*</sup> intermediate, which is formed via a barrierless pathway in both the forward and backward directions of the reaction, i.e.,  $\text{CH} + \text{H}_2 \rightleftharpoons \text{CH}_3^* \rightleftharpoons \text{CH}_2 + \text{H}$ . In the low-pressure regime, González et al. (2011) showed that the three hydrogen atoms become equivalent, as a result of the long-lived CH<sub>3</sub><sup>\*</sup> complex. In the high-pressure regime, on the other hand, McIlroy & Tully (1993) indicated that collisional stabilization to form ground-state CH<sub>3</sub> dominates. A reaction taking place on an ice surface can be seen as an extreme case of the high-pressure limit, in which the ice acts as a third body to take up the excess energy of the reaction (see Section 4.1 above). Given the barrierless nature of the PES, we expect no isotope effect here. In other words, it is highly likely that reaction (6) will lead barrierlessly to the formation of CH<sub>3</sub> on the ice, while reaction (9) is unlikely to take place at all and will revert simply to reaction (3), also forming CH<sub>3</sub>. This serves as an explanation why CH<sub>2</sub>D<sub>2</sub> is detected in experimental sets 1 and 2, since the barrierless nature leads to a lack of isotope effect.

#### 4.3. Hydrogen Abstraction Reactions

The two remaining reactions with molecular hydrogen, reactions (10) and (11), have been previously studied; the

**Table 3**  
Activation Energies from Predominantly Theoretical Chemical Literature for the Reactions (1)–(6) and (8)–(11) in kJ mol<sup>−1</sup>

Reaction		$\Delta E_{\text{act}}$	Ref.
(1)	${}^3\text{C} + \text{H} \rightarrow \text{CH}$	0	[1]
(2)	$\text{CH} + \text{H} \rightarrow \text{CH}_2$	0	[2]
(3)	${}^3\text{CH}_2 + \text{H} \rightarrow \text{CH}_3$	0	[3]
(4)	$\text{CH}_3 + \text{H} \rightarrow \text{CH}_4$	0	[4]
(5)	${}^3\text{C} + \text{H}_2 \rightarrow {}^3\text{CH}_2$	TBD <sup>a</sup>	[2]
(6)	$\text{CH} + \text{H}_2 \rightarrow \text{CH}_3$	0	[3]
(8)	$\text{CH} + \text{H} \rightarrow {}^3\text{C} + \text{H}_2$	− <sup>b</sup>	[2]
(9)	$\text{CH}_2 + \text{H} \rightarrow \text{CH} + \text{H}_2$	− <sup>c</sup>	[3]
(10)	${}^3\text{CH}_2 + \text{H}_2 \rightarrow \text{CH}_3 + \text{H}$	49	[5]
(11)	$\text{CH}_3 + \text{H}_2 \rightarrow \text{CH}_4 + \text{H}$	44	[6]

**Notes.** Note that reaction (7) can only take place in the singlet, excited, state, and is therefore excluded here.

<sup>a</sup> Cannot be trivially determined due to conical intersection and strong C–H<sub>2</sub>O interaction (see Section 4.1).

<sup>b</sup> The reaction is likely quenched in the CH<sub>2</sub> ground state (see Section 4.1 and Gamallo et al. 2012), effectively changing it to reaction (2).

<sup>c</sup> Reaction is determined by the relaxation of the CH<sub>3</sub><sup>\*</sup> intermediate (see Section 4.2) and thus leads to reaction (3).

**References.** [1] Qasim et al. (2020a); [2] Harding et al. (1993); van Harrevelt et al. (2002); Gamallo et al. (2012); this work; [3] McIlroy & Tully (1993); Medvedev et al. (2006); González et al. (2011); [4] Duchovic & Hase (1985); [5] Baskin et al. (1974); Bauschlicher (1978); [6] Li et al. (2015); Beyer et al. (2016).

reported barriers are presented in Table 3. Both reactions can only take place when a considerable barrier ( $> 44$  kJ mol<sup>−1</sup>) is overcome, for which tunneling needs to be invoked to reach rate constants that are high enough for the reaction to be able to take place at the low temperatures in dense molecular clouds. The effect of tunneling can be accurately included by means of instanton theory (Miller 1975; Langer 1976; Callan & Coleman 1977; Rommel & Kästner 2011; Richardson 2016). Although Beyer et al. (2016) indeed calculated instanton rate constants for the reaction  $\text{CH}_3 + \text{H}_2$ , they provided only bimolecular rate constants, whereas unimolecular rate constants are those relevant for Langmuir–Hinshelwood-type surface reactions (Lamberts et al. 2016; Meisner et al. 2017). Given the high activation barriers, about twice as large as for the reaction  $\text{H}_2 + \text{OH} \rightarrow \text{H}_2\text{O} + \text{H}$  (Meisner et al. 2017) and slightly above that of  $\text{H} + \text{H}_2\text{O}_2 \rightarrow \text{H}_2 + \text{HO}_2$  (Lamberts et al. 2016), relatively low rate constants are expected. As a consequence of the high barriers, these two reactions are expected to show significant kinetic isotope effects. This, in turn, explains why they are unlikely to take place with molecular deuterium. We interpret the lack of CD<sub>4</sub> detection in our experiments with only D<sub>2</sub> as a deuterium source as experimental confirmation that, indeed, tunneling plays a role in the abstraction reactions from molecular hydrogen and deuterium. A detailed quantitative study will be topic of a future study.

## 5. Astrochemical Implications and Conclusions

Currently, the main interstellar formation pathway of methane is thought to be through the reactions (1)–(4). Reactions (5), (10), and (11) are included in some astrochemical models, but in most studies the initial guesses by Hasegawa & Herbst are used; see for instance the current surface reactions in the KIDA database (Wakelam et al. 2015). Reaction (6),  $\text{CH} + \text{H}_2 \rightarrow \text{CH}_3$ , is usually not included at all.



For the interpretation of astronomical data, specifically those obtained by the JWST in the near future, it is important for models to take into account that:

1. the reaction  $C + H_2 \rightarrow CH_2$  is unlikely to proceed via a fully barrierless mechanism on water ices and an isotope effect is yet to be determined;
2. the reaction  $CH + H_2 \rightarrow CH_3$ , on the other hand, is expected to take place readily and barrierlessly without an isotope effect;
3. the abstraction reactions  $CH_2 + H_2 \rightarrow CH_3 + H$  and  $CH_3 + H_2 \rightarrow CH_4 + H$  take place via a tunneling mechanism and a pronounced isotope effect is expected.

The points above are summarized in Table 3 and Figure 4.

The main finding is that  $H_2$  plays a role in the solid-state formation of interstellar methane.  $CH_4$  can be formed without invoking any H atoms in our experiments, which is supported by our own calculations as well as theoretical results found in physical chemical literature. Thus, under physical conditions where  $H_2$  is much more abundant than H atoms and taking into account that  $H_2$  sticks to the surface at higher temperatures than H, methane formation from C atoms and  $H_2$  (HD,  $D_2$ ) molecules is a reaction route that should be taken into account. Both  $H_2$  and H abundances as well as their respective reaction efficiencies with carbon atoms determine the relative impact of both mechanisms, for which dedicated modeling will be needed. The finding that a  $C + H_2$  route also leads to methane formation has the following implications.

1. The formation of  $CH_4$  can take place at higher temperatures, e.g., 20 K instead of 10 K, because of the stronger binding of  $H_2$  molecules to the ice surface,
2.  $CH_4$  can be formed in the ice bulk through the interaction of entrapped  $H_2$  with  $CH_n$  radicals obtained by dissociation of hydrocarbons caused by UV photons or cosmic-ray particles,
3. Deuterium fractionation of methane is not only dictated by D/H ratios but also by (a) the respective abundances of  $D_2$  and HD with respect to  $H_2$  on the surface and (b) the higher abstraction rate constant of H atoms from  $H_2$ /HD compared to D abstraction from HD/ $D_2$ ; see for instance Figure 5,
4. While Qasim et al. (2020a) focused on confirming the atomic hydrogenation route of carbon to form  $CH_4$ , here we show that not only reactions with H, but also  $H_2$  chemistry overall, should be fully incorporated into astrochemical models. This is particularly true for models that include microscopic detail, despite the increase in computational cost.

We emphasize that astrochemical models are needed to study, in detail, the role of  $H_2$ , HD, and  $D_2$ , for the formation of methane isotopologues under dense cloud conditions.

T.L. is grateful for support from NWO via a VENI fellowship (722.017.008). G.F. acknowledges financial support from the Russian Ministry of Science and Higher Education via the State Assignment Contract FEUZ-2020-0038. This research benefited from the financial support from the Dutch Astrochemistry Network II (DANII). Further support includes a VICI grant of NWO (the Netherlands Organization for Scientific Research). Funding by NOVA (the Netherlands Research School for Astronomy) is acknowledged.

*Software:* Matplotlib (Hunter 2007), Numpy (van der Walt et al. 2011), Jupyter (Kluyver et al. 2016), Chemshell (Metz et al. 2014), Molpro (Werner et al. 2012).

## Appendix A Reaction Routes for the Formation of Methane Isotopologues

Below we explain the reaction pathways that lead to the formation of methane isotopologues of the form  $CH_nD_{4-n}$  with  $n=0-4$  in the experimental series 1–4. Please note that the reactions considered barrierless are reactions (1)–(4) and (6) and these are expected to take place without an isotope effect. Reaction (5) is likely possible both with  $H_2$  and  $D_2$ , although it is currently unclear whether the rate constant is determined by the change needed in electron configuration and/or a barrier on a water-rich surface. It is possible that the reaction is slower with  $D_2$ . Reactions (10) and (11) can only take place via tunneling and, given the high barrier, these reactions are expected to be very slow with  $D_2$ . In Figure 5 three networks are depicted, analogously to Figure 4, one for each deuteration experiment. As in Figure 4, three types of reactions are considered: H/D atom addition,  $H_2/D_2$  insertion, and  $H_2$  abstraction. Note that we deliberately choose not to include  $D_2$  abstraction reactions, because of the high barrier. Finally, we assume that the H or D atoms formed in situ do not take part in subsequent reactions, but desorb instead. We base this on the argument of conservation of energy and momentum (Koning et al. 2013).

The experiments are discussed below in order of increasing complexity.

### A.1. Experiments 3 and 4: $C + H_2$ and/or $D_2$

Experiment 4A with  $C + H_2$  leads clearly to the formation of  $CH_4$ , while experiment 3A with  $C + D_2$  does not lead to a  $CD_4$  detection. At the same time experiment 3B with  $C + H_2 + D_2$  shows the formation of  $CH_2D_2$  and  $CH_4$ , but not  $CD_4$ . This can be understood by considering the reactions presented in the top panel of Figure 5.

### A.2. Experiment 1: $C + H + H_2 + D_2$

Throughout the series for experiment 1 the only methane isotopologue species observed are  $CH_4$  and  $CH_2D_2$ . The reaction network in Figure 5 rationalizes these two detections by showing that these species can be formed via routes in which the majority of the reactions are barrierless. The formation of  $CHD_3$  or  $CH_3D$  (not depicted) would need to proceed through a  $+D_2$  tunneling abstraction reaction, which is unlikely to take place on laboratory timescales. Whether  $D_2$  abstraction on interstellar timescales depends on the competition with diffusion needs an astrochemical model for verification.

### A.3. Experiment 2: $C + H_2 + D + D_2$

In experimental series 2 we confirm the detection of  $CD_4$ ,  $CH_2D_2$ , and a tentative detection of  $CH_4$ . However, as can be seen from the reaction network in Figure 5, both  $CHD_3$  and  $CH_3D$  could be formed in principle. We attribute the lack of detection of these species to:

1. the existence of a fully barrierless formation pathway for both  $CD_4$  and  $CH_2D_2$ ,
2. the large band strength for  $CH_4$ , allowing a detection of small amounts,

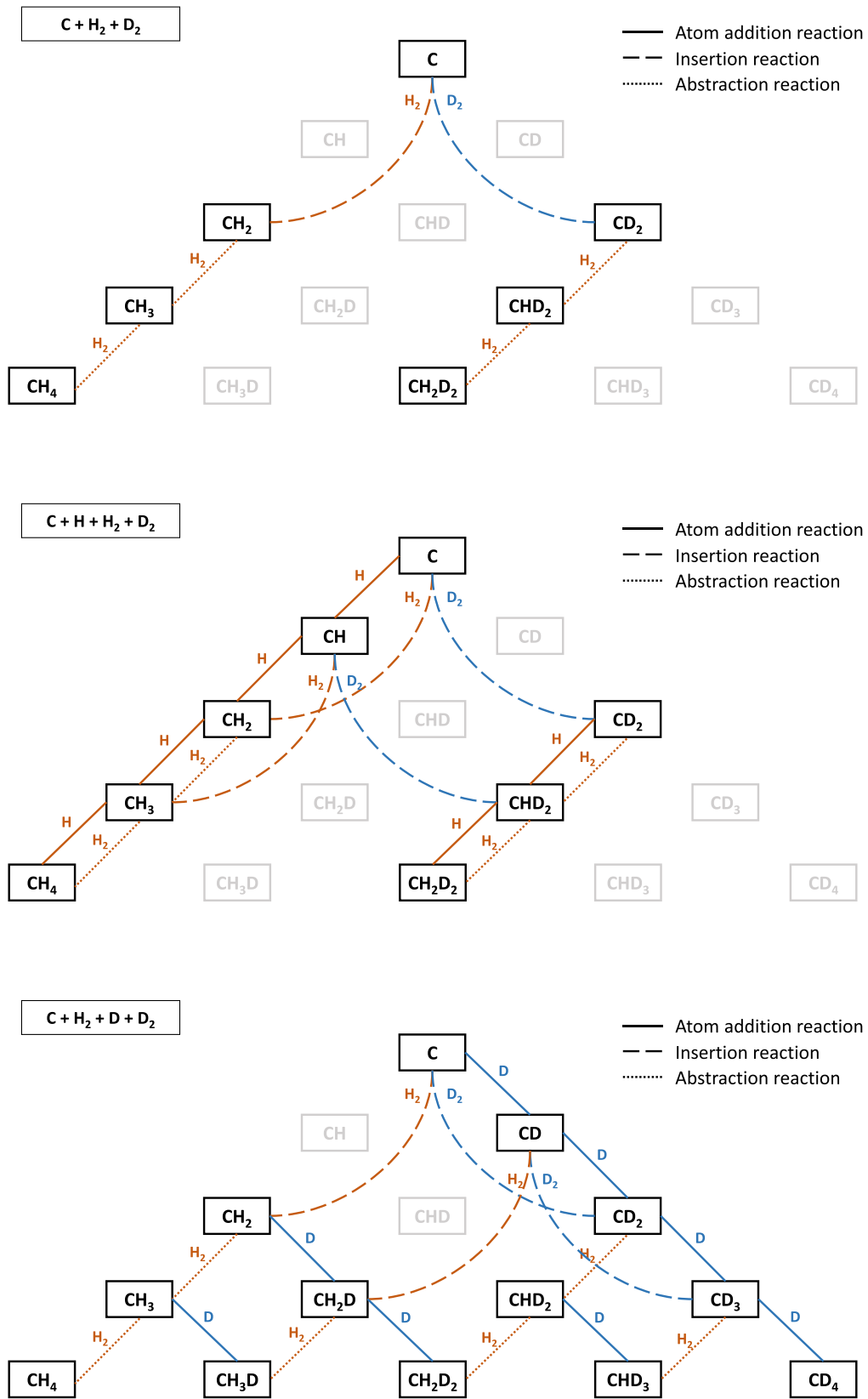


**Figure 5.** Reaction network for the hydrogenation and deuteration reactions leading to the formation of methane isotopologues. Analogously to Figure 4, three types of reactions are considered: H or D addition, H<sub>2</sub> or D<sub>2</sub> insertion, and H<sub>2</sub> abstraction.

3. the requirement for CHD<sub>3</sub> and CH<sub>3</sub>D of at least one reaction that involves tunneling of the type CH<sub>n</sub>D<sub>m</sub> + H<sub>2</sub>, which is in direct competition with a barrierless reaction of the type CH<sub>n</sub>D<sub>m</sub> + D.

For example, CH<sub>3</sub>D can be formed via three routes, all of which contain one reaction with a barrier:

1.	C + H <sub>2</sub> → CH <sub>2</sub>	CH <sub>2</sub> + H <sub>2</sub> → CH <sub>3</sub> + H	CH <sub>3</sub> + D → CH <sub>3</sub> D
2.	C + H <sub>2</sub> → CH <sub>2</sub>	CH <sub>2</sub> + D → CH <sub>2</sub> D	CH <sub>2</sub> D + H <sub>2</sub> → CH <sub>3</sub> D + H
3.	C + D → CD	CD + H <sub>2</sub> → CH <sub>2</sub> D	CH <sub>2</sub> D + H <sub>2</sub> → CH <sub>3</sub> D + H.

In contrast, CH<sub>2</sub>D<sub>2</sub> can be formed via four routes, of which route 3 is barrierless:

1.	C + H <sub>2</sub> → CH <sub>2</sub>	CH <sub>2</sub> + D → CH <sub>2</sub> D	CH <sub>2</sub> D + D → CH <sub>2</sub> D <sub>2</sub>
2.	C + D <sub>2</sub> → CD <sub>2</sub>	CD <sub>2</sub> + H <sub>2</sub> → CHD <sub>2</sub> + H	CHD <sub>2</sub> + H <sub>2</sub> → CH <sub>2</sub> D <sub>2</sub> + H
3.	C + D → CD	CD + H <sub>2</sub> → CH <sub>2</sub> D	CH <sub>2</sub> D + D → CH <sub>2</sub> D <sub>2</sub>
4.	C + D → CD	CD + D → CD <sub>2</sub>	CD <sub>2</sub> + H <sub>2</sub> → CHD <sub>2</sub> + H

## Appendix B Peak Positions and Detections

In Table 4 the observed peak positions are listed, along with their molecular assignment based on literature values. The last four columns indicate for which of the experiments a particular peak has been detected, with parentheses indicating a weak feature.

We confirm the results published by Qasim et al. (2020a), who showed that (deuterated) methane is efficiently formed when carbon atoms react with H (D) on a water surface via experiments 1A and 2A. Furthermore, we detect H<sub>2</sub>CO, CO<sub>2</sub>, and CO in situ in the solid state. Formaldehyde is present as a product from the reaction between the carbon atom and water (Hickson et al. 2016) and its formation is the topic of another recent study (Molpeceres et al. 2021). The presence of H<sub>2</sub>CO

further leads to the tentative detection of a CH<sub>3</sub>OH feature in experiments 1A and 1D at 1015 cm<sup>-1</sup> as a result of the hydrogenation of formaldehyde (Watanabe & Kouchi 2002; Fuchs et al. 2009; Qasim et al. 2018). Note that Fedoseev et al. (2022) showed that the reaction C + H<sub>2</sub>CO does not lead to a detectable amount of products using RAIRS, under similar experimental conditions, and therefore does not interfere with the reaction channels studied here. CO<sub>2</sub> is a contaminant that arises from atomic carbon sources of this design (Krasnokutski & Huisken 2014; Qasim et al. 2020b). Note also the gas-phase CO<sub>2</sub> bands around 2340 cm<sup>-1</sup>. Qasim et al. (2020b) showed that the reaction C + CO<sub>2</sub> has a high barrier and is unlikely to take place, and Bisschop et al. (2007) have shown that the reaction H + CO<sub>2</sub> also does not take place. CO deposition as a result of the source contamination takes place with a relatively high flux

**Table 4**  
Summary of All Detected Peak Positions, with the Exception of Water (H<sub>2</sub>O: 3380 and 1660 cm<sup>-1</sup> and D<sub>2</sub>O: 2440 and 1220 cm<sup>-1</sup>)

Peak pos. (cm <sup>-1</sup> )	Molecule	Reference	Detected in Exp. 1	Detected in Exp. 2	Detected in Exp. 3	Detected in Exp. 4
3007	CH <sub>4</sub>	[2]	1A, 1B	...	...	(4A)
3000	CH <sub>2</sub> D <sub>2</sub>	[3]	(1B), 1C	...	...	...
2343	CO <sub>2</sub>	[4]	All	All	3A, 3B	<sup>a</sup>
2277	CH <sub>2</sub> D <sub>2</sub>	[3]	1C	(2C)	...	...
2250	CD <sub>4</sub>	[5]	...	2A, 2B	...	...
2226	CH <sub>2</sub> D <sub>2</sub>	[3]	1C	...	...	...
2152	CO	[6]	All	All	3A, 3B	All
2137	CO	[6]	All	All	3A, 3B	All
1717	H <sub>2</sub> CO	[7]	All	All	3A, 3B	...
1666	D <sub>2</sub> CO	[8]	...	...	...	4A, 4B
1500	H <sub>2</sub> CO	[7]	All	All	3A, 3B	...
1430	CH <sub>2</sub> D <sub>2</sub>	[3]	1B, 1C	...	...	...
1303	CH <sub>4</sub>	[1, 2]	1A, 1B, (1C)	(2C)	(3B)	4A
1250	H <sub>2</sub> CO	[7]	1A	...	3A, 3B	...
1231	CH <sub>2</sub> D <sub>2</sub>	[3]	1B, (1B)	...	...	...
1102	D <sub>2</sub> CO	[8]	...	...	...	(4A), 4B
1083	CH <sub>2</sub> D <sub>2</sub>	[3]	1B,	(2C)	3B	...
1028	CH <sub>2</sub> D <sub>2</sub>	[3]	1B, (1B)	(2A), 2B, 2C	3B	...
1015	CH <sub>3</sub> OH	[9]	1A, (1B)	...	...	...
993	CD <sub>4</sub>	[5]	(1C)	2A, 2B, (2C)	...	...
991	D <sub>2</sub> CO	[8]	...	...	...	4A, 4B

**Notes.** Experiments in parentheses indicate a weak feature or tentative detection.

<sup>a</sup> Overlaps with the D<sub>2</sub>O stretch mode.

**References.** [1] Shimanouchi (1972); [2] Hagen et al. (1983); Quattrocci & Ewing (1992a); [3] Quattrocci & Ewing (1992b); [4] Gerakines et al. (1995); [5] Chapados & Cabana (1972); Edling et al. (1987); [6] Schmitt et al. (1989); [7] Schutte et al. (1996); [8] Tso & Lee (1984); Nagaoka et al. (2005); [9] Qasim et al. (2018).

of  $8 \times 10^{11} \text{ cm}^{-2} \text{ s}^{-1}$ , and subsequent reactions with H and C can lead to the formation of ketene (Fedoseev et al. 2022). This does not, however, interfere with the formation routes of methane since the reaction channels are separated. Finally, reactions between  $\text{H}_2\text{O}$  and  $\text{CH}_x$  radicals are not expected to play a role, because of the high barriers or endothermicity of the reaction involved (Jursic 1998; Tzeli & Mavridis 2005; Bergeat et al. 2009; Lamberts et al. 2017; Qasim et al. 2020a).

### Appendix C

#### Potential Energy Surfaces for the $\text{C}_{2v}$ and $\text{C}_s$ Symmetries

Figure 6 shows the potential energy cuts for the reaction  $\text{C} + \text{H}_2 \rightarrow \text{CH}_2$ , reaction (5), on both  $\text{C}_{2v}$  and  $\text{C}_s$  surfaces. Note that for both  $\text{C}_s$  surfaces at  $R > 1.8 \text{ \AA}$  we faced convergence issues. These values have been omitted. The position of the  $^3\text{CH}_2$  ground state is indicated in each figure.

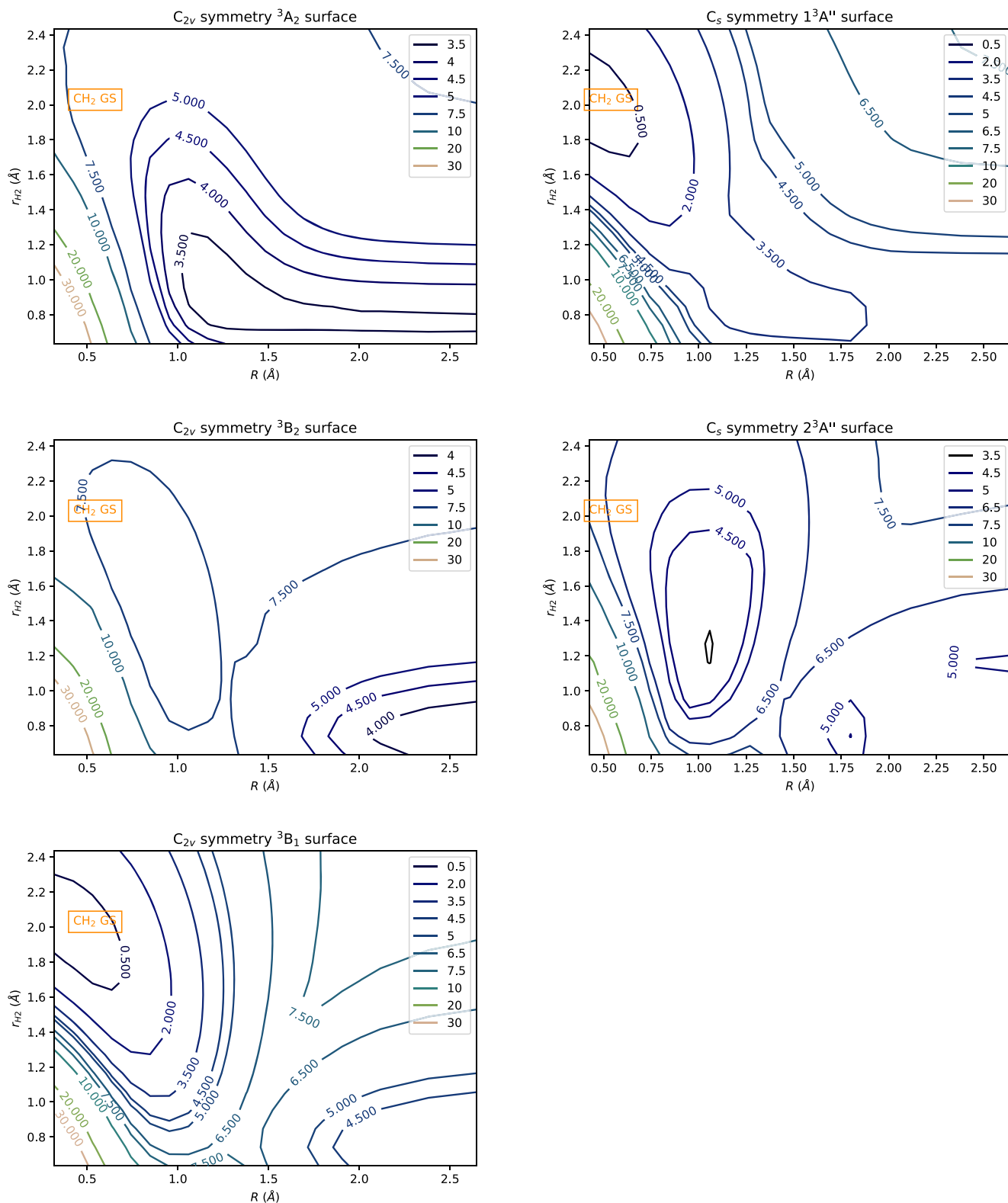


**Figure 6.** Potential energy cuts for the reaction  $C + H_2$  on three  $C_{2v}$  (left column) and two  $C_s$  symmetry (right column) surfaces. Contour units are in eV.

## ORCID iDs

Thanja Lamberts  <https://orcid.org/0000-0001-6705-2022>  
 Gleb Fedoseev  <https://orcid.org/0000-0003-2434-2219>  
 Danna Qasim  <https://orcid.org/0000-0002-3276-4780>  
 Ko-Ju Chuang  <https://orcid.org/0000-0001-6877-5046>  
 Julia C. Santos  <https://orcid.org/0000-0002-3401-5660>  
 Harold Linnartz  <https://orcid.org/0000-0002-8322-3538>

## References

- Adler, T. B., Knizia, G., & Werner, H.-J. 2007, *JChPh*, **127**, 221106  
 Albar, J. D., Summerfield, A., Cheng, T. S., et al. 2017, *NatSR*, **7**, 6598  
 Anton, R., Wiegner, T., Naumann, W., et al. 2000, *RSci*, **71**, 1177  
 Baskin, C. P., Bender, C. F., Bauschlicher, C. W., & Schaefer, H. F. 1974, *JChS*, **96**, 2709  
 Bauschlicher, C. W. 1978, *CPL*, **56**, 31  
 Bauschlicher, C. W., Haber, K., Schaefer, H. F., & Bender, C. F. 1977, *JChS*, **99**, 3610  
 Becke, A. D. 1988, *PhRvA*, **38**, 3098  
 Becke, A. D. 1993, *JChPh*, **98**, 5648  
 Bergat, A., Moisan, S., Méreau, R., & Loison, J.-C. 2009, *CPL*, **480**, 21  
 Beyer, A. N., Richardson, J. O., Knowles, P. J., Rommel, J., & Althorpe, S. C. 2016, *J. Phys. Chem. Lett.*, **7**, 4374  
 Bisbas, T. G., Schruha, A., & van Dishoeck, E. F. 2019, *MNRAS*, **485**, 3097  
 Bisschop, S. E., Fuchs, G. W., van Dishoeck, E. F., & Linnartz, H. 2007, *A&A*, **474**, 1061  
 Boogert, A. A., Gerakines, P. A., & Whittet, D. C. 2015, *ARA&A*, **53**, 541  
 Boogert, A. C. A., Schutte, W. A., Tielens, A. G. G. M., et al. 1996, *A&A*, **315**, L377  
 Brown, P. D., & Charnley, S. B. 1991, *MNRAS*, **249**, 69  
 Brown, P. D., Charnley, S. B., & Millar, T. J. 1988, *MNRAS*, **231**, 409  
 Burton, M. G., Ashley, M. C. B., Braiding, C., et al. 2015, *ApJ*, **811**, 13  
 Callan, C. G., & Coleman, S. 1977, *PhRvD*, **16**, 1762  
 Chapados, C., & Cabana, A. 1972, *CajCh*, **50**, 3521  
 Chuang, K. J., Fedoseev, G., Qasim, D., et al. 2018, *A&A*, **617**, A87  
 Cuppen, H. M., & Herbst, E. 2007, *ApJ*, **668**, 294  
 D'Hendecourt, L. B., Allamandola, L. J., & Greenberg, J. M. 1985, *A&A*, **152**, 130  
 Duchovic, R. J., & Hase, W. L. 1985, *JChPh*, **82**, 3599  
 Duflot, D., Toubin, C., & Monnerville, M. 2021, *FrASS*, **8**, 24  
 Dunning, T. H., Peterson, K. A., & Wilson, A. K. 2001, *JChPh*, **114**, 9244  
 Dunning, T. H. J. 1989, *JChPh*, **90**, 1007  
 Edling, J. A., Richardson, H. H., & Ewing, G. E. 1987, *JMoSt*, **157**, 167  
 Fedoseev, G., Qasim, D., Chuang, K.-J., et al. 2022, *ApJ*, **924**, 110  
 Fredon, A., Groenenboom, G. C., & Cuppen, H. M. 2021, *ESC*, **5**, 2032  
 Fuchs, G. W., Cuppen, H. M., Ioppolo, S., et al. 2009, *A&A*, **505**, 629  
 Furuya, K., Aikawa, Y., Hincelin, U., et al. 2015, *A&A*, **584**, A124  
 Gamallo, P., Defazio, P., Akpinar, S., & Petrongolo, C. 2012, *JPCA*, **116**, 8291  
 Garrod, R. T. 2013, *ApJ*, **778**, 158  
 Gerakines, P. A., Schutte, W. A., Greenberg, J. M., & van Dishoeck, E. F. 1995, *A&A*, **296**, 810  
 Goldsmith, P. F., & Li, D. 2005, *ApJ*, **622**, 938  
 González, M., Saracibar, A., & Garcia, E. 2011, *PCCP*, **13**, 3421  
 Greenler, R. G. 1966, *JChPh*, **44**, 310  
 Hagen, W., Tielens, A. G. G. M., & Greenberg, J. M. 1983, *A&AS*, **51**, 389  
 Harding, L., Guadagnini, R., & Schatz, G. 1993, *JPhCh*, **97**, 5472  
 Hasegawa, T. I., & Herbst, E. 1993, *MNRAS*, **261**, 83  
 Henning, T. K., & Krasnokutski, S. A. 2019, *NatAs*, **3**, 568  
 Hickson, K. M., Loison, J.-C., Lique, F., & Klos, J. 2016, *JPCA*, **120**, 2504  
 Hickson, K. M., Loison, J.-C., Nuñez-Reyes, D., & Méreau, R. 2016, *J. Phys. Chem. Lett.*, **7**, 3641  
 Hiraoka, K., Miyagoshi, T., Takayama, T., Yamamoto, K., & Kihara, Y. 1998, *ApJ*, **498**, 710  
 Hunter, J. D. 2007, *CSE*, **9**, 90  
 Ioppolo, S., Cuppen, H. M., Romanzin, C., van Dishoeck, E. F., & Linnartz, H. 2008, *ApJ*, **686**, 1474  
 Ioppolo, S., Fedoseev, G., Lamberts, T., Romanzin, C., & Linnartz, H. 2013, *RSci*, **84**, 073112  
 Janssen, C. L., & Nielsen, I. M. 1998, *CPL*, **290**, 423  
 Jursic, B. S. 1998, *JPCA*, **102**, 9255  
 Kästner, J., Carr, J. M., Keal, T. W., et al. 2009, *JPCA*, **113**, 11856  
 Keene, J., Blake, G. A., Phillips, T. G., Huggins, P. J., & Beichman, C. A. 1985, *ApJ*, **299**, 967  
 Kendall, R. A., Dunning, T. H., & Harrison, R. J. 1992, *JChPh*, **96**, 6796  
 Kim, G.-S., Nguyen, T. L., Mebel, A. M., Lin, S. H., & Nguyen, M. T. 2003, *JPCA*, **107**, 1788  
 Kluyver, T., Ragan-Kelley, B., Pérez, F., et al. 2016, in *Positioning and Power in Academic Publishing: Players, Agents and Agendas*, ed. F. Loizides & B. Schmidt (Amsterdam: IOS Press), 87  
 Knizia, G., Adler, T. B., & Werner, H.-J. 2009, *JChPh*, **130**, 054104  
 Koning, J., Kroes, G. J., & Arasa, C. 2013, *JChPh*, **138**, 104701  
 Krasnokutski, S. A., & Huisken, F. 2014, *ApPhL*, **105**, 113506  
 Krasnokutski, S. A., Kuhn, M., Renzler, M., et al. 2016, *ApJL*, **818**, L31  
 Lacy, J. H., Carr, J. S., Evans, N. J. I., et al. 1991, *ApJ*, **376**, 556  
 Lambert, N., Kaltsoyannis, N., Price, S. D., Žabka, J., & Herman, Z. 2006, *JPCA*, **110**, 2898  
 Lamberts, T., Cuppen, H. M., Ioppolo, S., & Linnartz, H. 2013, *PCCP*, **15**, 8287  
 Lamberts, T., Fedoseev, G., Kästner, J., Ioppolo, S., & Linnartz, H. 2017, *A&A*, **599**, A132  
 Lamberts, T., Samanta, P. K., Köhn, A., & Kästner, J. 2016, *PCCP*, **18**, 33021  
 Langer, W. 1976, *ApJ*, **206**, 699  
 Lee, C., Yang, W., & Parr, R. G. 1988, *PhRvB*, **37**, 785  
 Li, J., Chen, J., Zhao, Z., et al. 2015, *JChPh*, **142**, 204302  
 McIlroy, A., & Tully, F. P. 1993, *JChPh*, **99**, 3597  
 Medvedev, D. M., Harding, L. B., & Gray, S. K. 2006, *MolPh*, **104**, 73  
 Meisner, J., Lamberts, T., & Kästner, J. 2017, *ESC*, **1**, 399  
 Metz, S., Kästner, J., Sokol, A. A., Keal, T. W., & Sherwood, P. 2014, *Wiley Interdiscip. Rev. Comput. Mol. Sci.*, **4**, 101  
 Miller, K. J. 1975, *JChPh*, **62**, 1759  
 Miyauchi, N., Hidaka, H., Chigai, T., et al. 2008, *CPL*, **456**, 27  
 Molpeceres, G., Kästner, J., Fedoseev, G., et al. 2021, *J. Phys. Chem. Lett.*, **12**, 10854  
 Molpeceres, G., Zaverkin, V., & Kästner, J. 2020, *MNRAS*, **499**, 1373  
 Murrell, J. N., Pedley, J. B., & Durmaz, S. 1973, *J. Chem. Soc., Faraday Trans.*, **2**, 1370  
 Nagaoka, A., Watanabe, N., & Kouchi, A. 2005, *ApJL*, **624**, L29  
 Öberg, K. I., Boogert, A. C. A., Pontoppidan, K. M., et al. 2008, *ApJ*, **678**, 1032  
 Papadopoulos, P. P., Thi, W. F., & Viti, S. 2004, *MNRAS*, **351**, 147  
 Peterson, K. A., Adler, T. B., & Werner, H.-J. 2008, *JChPh*, **128**, 084102  
 Qasim, D., Chuang, K.-J., Fedoseev, G., et al. 2018, *A&A*, **612**, A83  
 Qasim, D., Fedoseev, G., Chuang, K. J., et al. 2020a, *NatAs*, **4**, 781  
 Qasim, D., Witlox, M. J. A., Fedoseev, G., et al. 2020b, *RSci*, **91**, 054510  
 Quattrocchi, L. M., & Ewing, G. E. 1992a, *JChPh*, **96**, 4205  
 Quattrocchi, L. M., & Ewing, G. E. 1992b, *CPL*, **197**, 308  
 Richardson, J. O. 2016, *JChPh*, **144**, 114106  
 Rommel, J. B., & Kästner, J. 2011, *JChPh*, **134**, 184107  
 Schmidt, A., Offermann, J., & Anton, R. 1996, *TSF*, **281**, 105  
 Schmitt, B., Greenberg, J. M., & Grim, R. J. A. 1989, *ApJL*, **340**, L33  
 Schutte, W. A., Gerakines, P. A., Geballe, T. R., van Dishoeck, E. F., & Greenberg, J. M. 1996, *A&A*, **309**, 633  
 Shimanouchi, T. 1972, *Nat. Stand. Ref. Data Ser. Nat. Bur. Stand.*, **1**, 39  
 Simonishi, T., Nakatani, N., Furuya, K., & Hama, T. 2018, *ApJ*, **855**, 27  
 Simončić, M., Semenov, D., Krasnokutski, S., Henning, T., & Jäger, C. 2020, *A&A*, **637**, A72  
 Snow, T. P., & McCall, B. J. 2006, *ARA&A*, **44**, 367  
 Tso, T. L., & Lee, E. K. C. 1984, *JPhCh*, **88**, 5475  
 Tzeli, D., & Mavridis, A. 2005, *IJCQ*, **104**, 497  
 van de Hulst, H. C. 1946, *RAOU*, **11**, 2  
 van de Hulst, H. C. 1949, *The Solid Particles in Interstellar Space* (Utrecht: Drukkerij Schotanus & Jens)  
 van der Walt, S., Colbert, S. C., & Varoquaux, G. 2011, *CSE*, **13**, 22  
 van Dishoeck, E. F., & Black, J. H. 1988, *ApJ*, **334**, 771  
 van Harreveld, R., van Hemert, M. C., & Schatz, G. C. 2002, *JChPh*, **116**, 6002  
 Vasyunin, A. I., & Herbst, E. 2013, *ApJ*, **762**, 86  
 Wakelam, V., Loison, J. C., Herbst, E., et al. 2015, *ApJS*, **217**, 20  
 Wakelam, V., Loison, J. C., Mereau, R., & Ruaud, M. 2017, *MolAs*, **6**, 22  
 Watanabe, N., & Kouchi, A. 2002, *ApJL*, **571**, L173  
 Weigend, F., & Ahlrichs, R. 2005, *PCCP*, **7**, 3297  
 Werner, H., & Knowles, P. J. 1988, *JChPh*, **89**, 5803  
 Werner, H.-J., Knowles, P. J., Knizia, G., et al. 2018, *MOLPRO*, v2018.1, a package of ab initio programs, <https://www.molpro.net/>  
 Werner, H.-J., Knowles, P. J., Knizia, G., Manby, F. R., & Schütz, M. 2012, *WIRES Comput. Mol. Sci.*, **2**, 242  
 Werner, H.-J., Knowles, P. J., Manby, F. R., et al. 2020, *JChPh*, **152**, 144107  
 Woon, D. E., & Dunning, T. H. 1993, *JChPh*, **98**, 1358